Supporting Information

Text S1. Analytical methods

The pH of solutions was measured using a pH meter (FE28, Mettler-Toledo, Switzerland), while the sludge slurry conductivity was measured by a conductivity meter (DDS-307A, Shanghai Leici Instrument Factory, China). The samples were centrifuged using a high-speed centrifuge (5804R, Eppendorf, Germany) at 10000 r/min for 10 min, and the supernatant was promptly analyzed as a soluble fraction. Conventional parameters, such as TS, VS, NH_4^+, SCOD, proteins and polysaccharides, Fe^{2+} and Fe^{3+} were quantified following established protocols outlined in prior studies (Li et al., 2021b). Additionally, biogas was collected from reactors using a 0.2 L airbag (Dalian Haide Gas Sampling Bag Co., Ltd., China), and its specific volume was measured daily via extraction with a graduated syringe. A gas chromatograph (GC7890A, Agilent Technologies, USA) equipped with a thermal conductivity detector (TCD) and flame ionization detector (FID) was used to analyze the biogas composition. For the determination of VFAs in the slurry, the soluble fraction of the sample was filtered through a 0.45-μm microfiber filter (Tianjin Jinteng Experimental Equipment Co., Ltd., China), and the filtrate was determined using a gas chromatograph (GC7890A, Agilent Technologies, USA) equipped with a flame ionization detector and a HP-INNOWax capillary column (30 m × 0.25 mm × 0.25 μm).

Text S2. Characterization of cyclic voltammetry (CV), sludge conductivity, and ETS measurement

The CV experiments were performed using a single-chamber three-electrode electrochemical cell to characterize redox reactions in anaerobic reactions (Liu et al., 2022). The electrochemical cell was equipped with a graphite electrode (working electrode) of 75 mm length and 6 mm diameter, a Pt electrode (counter electrode) of 10*10*100 mm dimensions and a reference electrode (Ag/AgCl). Amounts of 50 mL sludge was abstracted from each reactor and poured into the electrochemical cell and the cell headspace was purged with N_2 for 5 min. The CV test was then performed in the range of -0.8–1.0 V (relative to Ag/AgCl) at a scan rate of 50 mV/s using an electrochemical workstation (CHI 660E, Huachen Instruments, China). The quantity of transferred electrons was evaluated by integrating the current–time curve from the CV voltammogram. The electron acceptor capacity (EAC), electron donor capacity (EDC) and electron transfer capacity (ETC) were calculated using the following equations:

$$EAC = \int I_{red}\, dt/F$$

$$EDC = \int I_{ox}\, dt/F$$

$$ETC = EAC + EDC$$

where I_{red} and I_{ox} are the reductive and oxidative currents in the sludge sample (A), respectively, F=96485.33 (C/mol e^-), t is the duration time of the current peak (s).

To compare the conductivity of the suspended sludge after the 30 day experiments, a three-probe electrical conductance measurement was performed with

two platinum electrodes separated by a 1 mm non-conductive gap (Zhu et al., 2023). Briefly, the sludge taken from the anaerobic system was subjected to centrifugation at 10000 r/min for 10 min and then washed three times by 0.1 mol/L NaCl solution (≥ 99% purity, Sinopharm Chemical Reagent Co., Ltd., China). Subsequently, the suspended sludge samples were placed in the 1 mm non-conductive gap between the two gold electrodes. A voltage ramp of −0.3–+0.3 V across split electrodes in steps of 0.025 V was applied by an electrochemical workstation. For each measurement, after allowing the exponential decay of transient ionic current, the steady-state electronic current for each voltage was measured every second over a minimum period of 120 s. The time-averaged current for each applied voltage was recorded to create the current−voltage curve. The conductivity of sludge was calculated by the following equation:

$$\sigma = L/RS$$

where σ is the sludge conductivity (μS/cm), L is the width of the gap (cm), R is the reciprocal of the slope in the current-voltage curve (Ω), S is the cross-sectional area (cm^2).

The ETS activities of sludge were measured by the INT-ETS method with a slight modification (Yin et al., 2018). The ETS activity is evaluated by analyzing the respiratory activity of microorganisms to evaluate the biological activity of the sludge, which is measured by the INT (2-(p-iodophenyl)-3-(p-nitrophenyl)-5-phenyltetrazolium chloride, ≥95%, Sigma-Aldrich, USA) method. In brief, 0.5 mL of sludge sample, 1.5 mL of Tris-HCl (pH 8.4, Beijing Solarbio Science &

Technology Co., Ltd., China), and 1.0 mL of INT (0.2%) were mixed in a 10 mL centrifuge tube. The reaction was carried out at 37℃ for 30 min in the dark using a thermostatic shaker (ZWY-1102C, Shanghai Zhicheng Analytical Instrument Manufacturing Co., Ltd., China) at 120 r/min. Subsequently, 1 mL of formaldehyde solution (37 wt%, Macklin Biochemical Co., Ltd., China) was added to terminate the enzymatic reaction. Then, 5 mL of methanol (≥99.5%, Macklin Biochemical Co., Ltd., China) were added and incubated at 37℃ for 10 min under the same shaking conditions. Lastly, the samples were centrifugated at 5000 g for 5 min and the absorbance was determined at 485 nm using a spectrometer (DR6000, Hach Company, USA).

The equation used to calculate the ETS activity was adapted by substituting the weight of sludge with the volume of mixed liquor, as follows:

$$U = \frac{D_{485} V_e}{\mathrm{K} V_t}$$

where U is the ETS activity (μg/mL·min), D_{485} is the absorbance at 485 nm, V_e is the volume of extractant (mL), K is the slope of the standard curve, V_t is the volume of mixed liquor (mL) at an incubation time of t (min).

Text S3. Description of the modified Gompertz model

The modified Gompertz model for cumulative methane yield was applied to quantitatively analyze the production of CH_4 under various conditions (Qin et al., 2017), as follows:

$$P = P_{max} exp\{-exp[R_{max} e(\lambda - t)/P_{max} + 1]\}$$

where P is the cumulative methane yield at time t (mL), P_{max} is the maximum cumulative methane yield (mL), R_{max} is the maximum methane yield rate (mL/days), e is 2.71828, λ is the lag phase (days), and t is the Co-AD reaction time (days).

Table S1 shows the calculated parameters such as the simulative cumulative methane yield (P_{max}, mL), maximum methane production rate (R_{max}, mL/days) and the lag phase time (λ, days). The R^2 values of the modified Gompertz model ranged from 0.96 to 0.998, indicating that the model can accurately describe the change in Co-AD gas production (Li et al., 2021a). The simulated cumulative methane yield was found to be in good agreement with the experimental results, suggesting that the modified Gompertz model can effectively describe methanogenesis.

Table S1. The model estimation results from the modified Gompertz model. Note: Slu refers to sludge anaerobic digestion, and the Co refers to sludge and bacterial residue co-digestion

Group	P_{max} (mL/ g VS)	R_{max} (mL/days)	λ (days)	R^2
Co-Control	111.93 ± 8.27	12.01 ± 0.61	4.15 ± 0.15	0.98
Co-Fe^0 NPs	148.85 ± 14.29	14.46 ± 1.04	4.50 ± 0.19	0.97
Co-$Fe^{2+/3+}$ NPs	133.24 ± 4.62	15.99 ± 0.44	4.10 ± 0.08	0.99
Co-Fe^{3+} NPs	163.64 ± 11.78	17.49 ± 0.96	4.39 ± 0.12	0.98

Text S4. The description of microbial community measurement in this study

For 16S rRNA high-throughout sequencing, DNA extraction was performed using a DNA extraction Kit (E.Z.N.A.® Soil DNA Kit, Omega bio-tek, USA). PCR was used to amplify the V3−V4 region of the bacterial 16S ribosomal RNA gene using primers 338F (5'−ACTCCTACGGGAGGCAGCAG−3') and 806R (5'−

GGACTACHVGGGTWTCTAAT−3'), and the V4−V5 region of the archaea was amplified by 524F (5′−TGYCAGCCGCCGCGGTAA−3′) and Arch958R (5′−YCCGGCGTTGAVTCCAATT−3′). The amplified products were purified and quantified, and sequenced using Majorbio's Illumina MiSeq PE300 according to the standard protocols.

For metagenomics sequencing, DNA extract was fragmented to an average size of about 350 bp using Covaris M220 (Gene Company Limited, China) for paired-end library construction. The paired-end library was constructed using NEXTFLEX Rapid DNA-Seq (Bioo Scientific, Austin, TX, USA). Paired-end sequencing was performed on Illumina NovaSeq™ X Plus (Illumina Inc., San Diego, CA, USA) at Majorbio Bio-Pharm Technology Co., Ltd. (Shanghai, China) using NovaSeq X Series 25B Reagent Kit according to the manufacturer's instructions (www.illumina.com).

The sequencing data of microbial community structure and diversity was processed on the free online Majorbio Cloud Platform (www.majorbio.com). To further estimate the function and metabolic pathway of genes, the Cluster of orthologous groups of proteins (COG) annotation for the representative sequences were conducted via Diamond against the EggNOG database (version 5.0). The Kyoto Encyclopedia of Genes and Genomes (KEGG) was performed using Diamond against the KEGG database.

Text S5. Characterization of Fe-NPs

The specific surface area and surface charge properties of Fe NPs were characterized. BET analysis revealed that Fe^0 NPs had a specific surface area of 4.02 m^2/g, while $Fe^{2+/3+}$ NPs and Fe^{3+} NPs exhibited larger surface areas of 8.13 m^2/g and 7.59 m^2/g, respectively. The point of zero charge (pH_{PZC}) of Fe-NPs was determined based on the Boltzmann distribution model, and the values were determined to be 6.86 for Fe^0 NPs, 5.55 for $Fe^{2+/3+}$ NPs, and 7.48 for Fe^{3+} NPs. These physicochemical properties suggest that the Fe oxides, especially Fe^{3+} NPs, provide more accessible reactive sites and near-neutral surface conditions, which may facilitate microbial interactions and electron transfer in the co-digestion process.

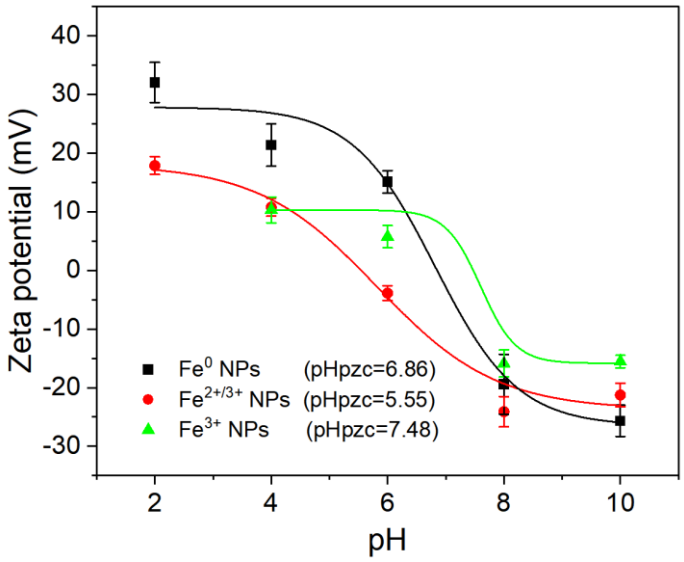

Fig. S1. Point of zero charge (pH_{PZC}) of Fe-NPs based on the Boltzmann distribution model

Text S6. Variation of evolution of dissolved organic matter (DOM) with varying-valence state addition to the Co-AD system

Prior to EEM measurement, the sludge supernatant underwent dilution to prevent

fluorescence quenching caused by the high organic matter concentration. Distilled water served as a blank for correction to mitigate the effects of Raman scattering and ensure the comparability of spectra.

In the 3D fluorescence spectrum, five regions delineate distinct substances based on the excitation and emission wavelengths. On day 2 of fermentation, the fluorescence intensity in these regions surpassed that of the control group in Fe^0 NPs, $Fe^{2+/3+}$ NPs and Fe^{3+} NPs groups (Fig. S2a), indicating enhanced sludge decomposition and organic matter release. Region IV, corresponding to dissolved metabolites, dominated the Co-AD system, followed by tryptophan-like substances in region II. Regions I and IV typically comprise biodegradable organics, while the remaining regions contain non-biodegradable organics. Fe^{3+} NPs notably augmented the biodegradability of refractory substances by microbial-mediated insoluble Fe(III) metabolism.

The fluorescence response integral of each region can serve as a representation of the respective organic matter content. The percent fluorescence response ($P_{i,n}$) of DOM from different stages of control, Fe^0 NPs, $Fe^{2+/3+}$ NPs and Fe^{3+} NPs groups are shown in Fig. S2b. Initially, region IV accounted for approximately 32%–34% of the total, gradually diminishing to 16%–18%, and then further to 13%–15% in the late digestion stage. Similarly, region II exhibited a consistent trend, stabilizing at 40%–42% and later at 33%. This suggests continual microbial utilization of soluble microbial by-products and tryptophan-like proteins for methane conversion, with Fe^{3+} NPs accelerating this process. Interestingly, the proportion of region I and region III

increased during digestion, reflecting the accumulation of non-degradable organics typical in sludge AD (Zhang et al., 2017). Region V, representing humic acid-like organics, remained consistently minimal, indicating limited anaerobic biodegradability.

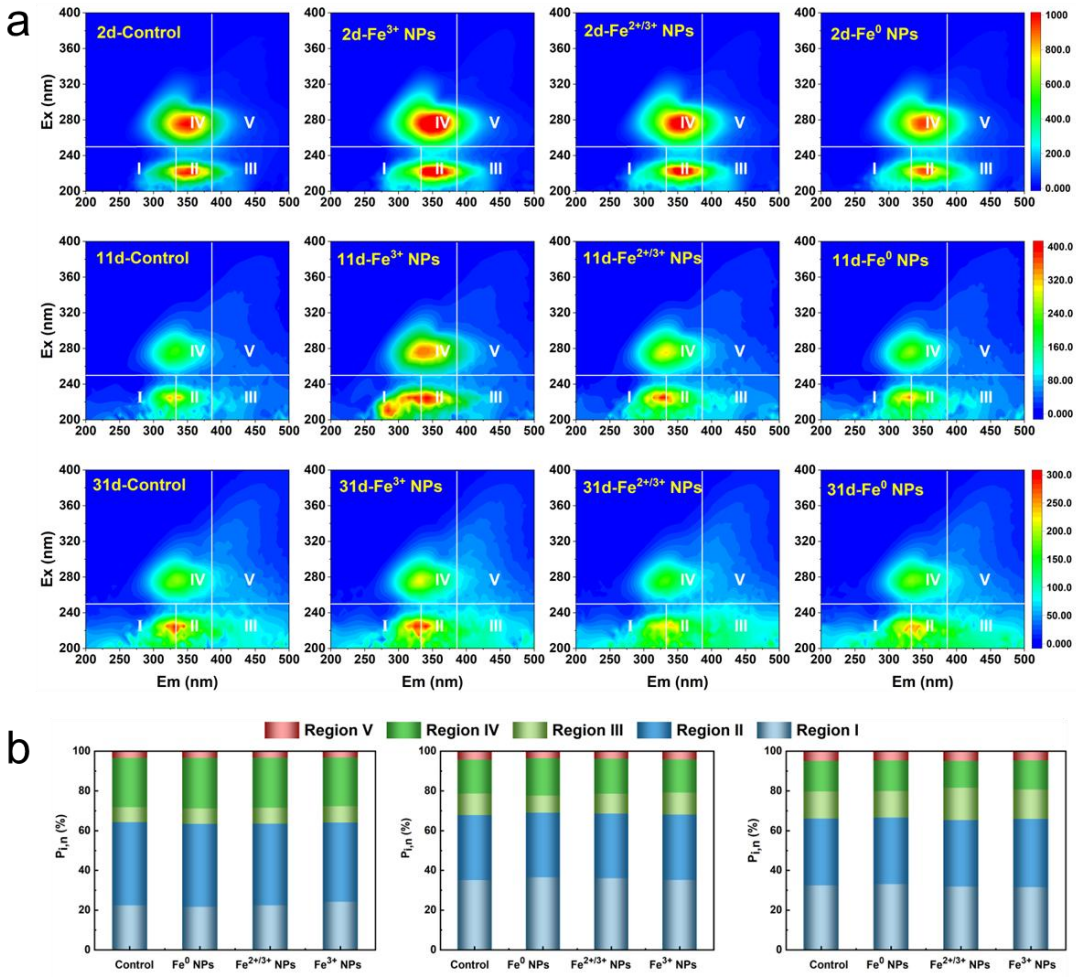

Fig. S2. (a) 3D-EEM spectra of sludge supernatant with digestion reaction and (b) the corresponding fluorescence region integral ratio of 3D-EEM spectrum.

Text S7. The description of richness and diversity of bacteria and archaea on the Co-AD system

Table S2 displays the bacterial community richness and diversity in samples obtained from the four tests. The bacterial community demonstrated higher richness and diversity than archaea. Coverage reflects the community coverage, with a larger value indicating a higher probability of detecting microbial sample sequences in sludge. The coverage values of the four samples all exceeded 99.6%, implying that the results of those sequencing tests could represent the real situations well. Ace and Chao reflect microbial richness and both values are positively proportional to species diversity. The Ace and Chao indices of Fe^0 NPs, $Fe^{2+/3+}$ NPs and Fe^{3+} NPs were all lower than those of the control group. The bacterial richness gradually decreased with the increase of valence state of the Fe NPs material. The Shannon and Simpson indices were used to estimate alpha diversity in the microbial communities in sludge samples. The Shannon value was positively correlated with species diversity, while the Simpson value was negatively correlated with species diversity. The diversity of Fe^0 NPs was the highest, followed by the control group. The addition of $Fe^{2+/3+}$ NPs and Fe^{3+} NPs reduced the diversity of bacteria. This is due to the selective competitive pressure of $Fe^{2+/3+}$ NPs and Fe^{3+} NPs on functional microorganisms in the digestive system, leading to a decline in the species diversity index. From the richness and diversity index of bacteria, it is evident that the addition of Fe NPs has a certain effect on the growth and metabolism of bacterial community. Furthermore, high-valence Fe NPs additives exhibit a more severe toxic effect on microbial cells.

Table S2. Bacterial community richness and diversity index

Sample/Estimators	Coverage	Ace	Chao	Shannon	Simpson
Control	0.9960	761.0138	760.0612	3.723051	0.100219
Fe^{0}	0.9968	744.0103	734.6471	4.027371	0.059571
$Fe^{2+/3+}$ NPs	0.9963	741.38	736.4845	3.711465	0.084233
Fe^{3+} NPs	0.9962	730.0946	724.15	3.580379	0.110078

Table S3 presents the diversity indices of the archaea community in the four reactors. Unlike the abundance of bacteria, the Ace and Chao indexes of the Fe^{3+} NPs group were the largest, followed by $Fe^{2+/3+}$ NPs, suggesting that the addition of $Fe^{2+/3+}$ NPs and Fe^{3+} NPs enhanced the growth and reproduction of archaea, leading to an increase in the total number of the archaea community. This trend also corresponds to methane production. The richness of the methanogenic archaea community in the Fe^{3+} NPs group was the highest, so the methane production was also the highest. However, the abundance of Fe^{0} NPs was lower than that of the control group, possibly due to the cytotoxicity of Fe^{0} NPs. The Fe^{0} NPs have strong reducibility and can react with key functional proteins on the cell membrane, thus damaging the integrity of the cell membrane. The Shannon and Simpson indices showed that the archaea diversity of the Fe^{3+} NPs was significantly lower than that of the other three groups, implying that the addition of Fe^{3+} NPs enriched the dominant methanogens and reduced the archaea diversity. However, the archaea diversity of $Fe^{2+/3+}$ NPs and Fe^{0} NPs were higher than that of the control group, likely due to the low-cost Fe NPs providing the trace element Fe necessary for microbial growth, which is conducive to the synthesis of microbial cells and the increase in the diversity of the archaea community.

Table S3. Archaea community richness and diversity index

Sample/Estimators	Coverage	Ace	Chao	Shannon	Simpson
Control	0.999963	25.29786	25	1.293803	0.369584
Fe^0	0.999963	23.34911	23	1.446814	0.302967
$Fe^{2+/3+}$ NPs	0.999889	27.6602	26.5	1.440857	0.334229
Fe^{3+} NPs	0.999889	28.32	27	0.783069	0.693142

Text S8. Metabolism pathway with varying-valence state Fe NPs addition on Co-digestion

The microbial metabolic functional abundance based on the Cluster of Orthologous Groups (COG) classification for the four reactors is depicted in Fig. S3a and S3b. Higher abundances of 19 functional metabolic genes were observed, particularly in energy production and conversion, amino acid transport and metabolism, coenzyme transport and metabolism, translation abundance related to ribosomal structure and biogenesis and inorganic ion transport and metabolism. This indicated the importance of material transport and energy metabolism in all reactors. Bacterial metabolic abundances were generally lower in Fe-based material groups compared to the control, indicating Fe NPs addition consumes organic matter early in digestion. In the later stages, virtually all VFAs were completely degraded, leading to a decrease in bacterial activity levels within the anaerobic system. However, Fe^{3+} NPs maintained favorable bacterial metabolic levels. For archaea, the Fe^{3+} NPs showed higher energy production and conversion, as well as coenzyme transport and

metabolism, closely correlating with methane generation. Therefore, the Fe^{3+} NPs materials can enhance the methane generation pathway, elevating these metabolic functions.

The KEGG pathway database categorizes biological metabolic pathways into 6 categories (level 1), including Metabolism, Genetic Information Processing, Environmental Information Processing, Cellular Processes, Human Diseases and Organismal Systems, and Metabolism was the main metabolic pathway in all four groups. Within the Metabolism, 13 pathway functions (level 2) were identified, with Energy metabolism, Carbohydrate metabolism, Amino acid metabolism and Lipid metabolism annotations yielding the highest number of genes in the four groups (Fig. S3c and S3d). Bacterial metabolism levels did not differ significantly among the groups. Regarding archaea, the Fe^{3+} NPs group showed the highest abundances in Energy metabolism, Methane metabolism and Carbon fixation pathways in prokaryotes (level 3), followed by the $Fe^{2+/3+}$ NPs group. This suggests that Fe^{3+} NPs and $Fe^{2+/3+}$ NPs enhance carbon fixation and methane generation. However, for Carbohydrate metabolism, Amino acid metabolism and Lipid metabolism pathways, Fe NPs addition led to reduced abundances, indicating no improvement in the hydrolytic acidification pathway.

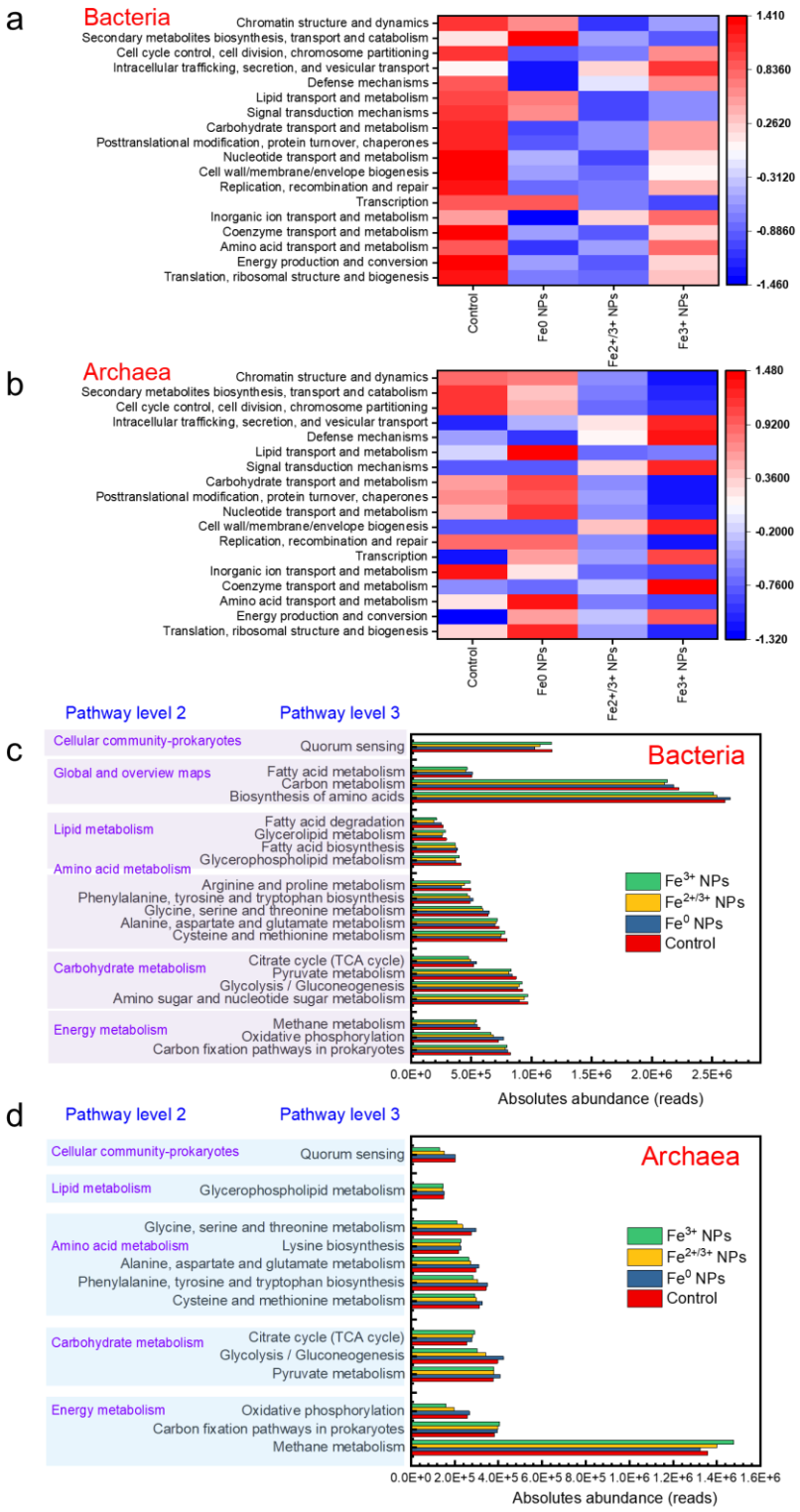

Fig. S3. Variation in microbial function profiles during co-digestion with Fe NPs addition analyzed by PICRUSt 2: (a) bacteria and (b) archaea on COG pathway, (c) bacteria and (d) archaea on KEGG pathway.

Table S4. The relative abundance of key genes involved in acidogenesis

Pathways	Ko number	Gene name	Abundance (reads)			
			Control	Fe^0 NPs	$Fe^{2+/3+}$ NPs	Fe^{3+} NPs
Glycolysis	K00844	*hk*	43.75	70.85	105.35	112.75
	K00886	*ppgk*	1302.83	992.83	948.16	1094.5
	K00845	*glk*	43197.84	44268.36	45723.34	42869.5
	K00918	*pfkC*	16	21.5	6	1.5
	K01810	*gpi*	28588.13	28511.15	28572.32	28418.56
	K06859	*pgi1*	108	123.5	132	43.5
	K13810	*tal-pgi*	1462	1788.5	1409	1253
	K15916	*pgi-pmi*	2414	4382.5	5242.5	3896.5
	K00850	*pfkA*	40056.51	40680.81	44036.37	42421.84
	K16370	*pfkB*	347.2	288.1	236.8	248.25
	K00918	*pfkC*	16	21.5	6	1.5
	K01624	*fbaA*	28939.2	28322.1	28904.74	28630.43
	K11645	*fbaB*	2730.95	5542.85	5994.55	3943.25
	K01623	*aldo*	586.5	514.5	469	604.25
	K01803	*tpiA*	30792.38	31185.15	31631.82	30844.56
	K00134	*gapA*	44173.08	40858.93	40191.81	42038.97
	K00150	*gap2*	18.5	23.5	7.5	6
	K00927	*pgk*	29838.63	29965.65	29976.82	29623.56
	K01834	*gpmA*	7908.44	8442.59	8073.61	7934.75
	K15634	*gpmB*	34461.96	31550.65	34266.73	37242.81
	K15633	*gpml*	23860.72	20940.83	20013.84	21719.48
	K15635	*apgm*	4602.33	7995.74	8869.82	6066.83
	K00131	*gapN*	3492.5	2544.77	3514.5	4290.51
	K01689	*eno*	29795.38	29888.4	29682.4	29595.81
	K00873	*pyk*	33198.19	31796.55	35097.48	35843.79

	K00163	*aceE*	5025.53	4643.34	2009.54	2762.33
	K00161	*pdhA*	10524	16487	16258.34	12804.41
	K00162	*pdhB*	9616.5	13888	12273.84	10109.91
	K00627	*pdhC*	14446.83	19930.46	15357.84	11521.67
Pyruvate	K00382	*pdhD*	40261.34	40561.14	33894.77	33057.82
metabolism	K00169	*porA*	1184.5	1450.5	2141.5	1924.5
	K00170	*porB*	1277	1569	2262	2007.5
	K00172	*porC*	1201	1451	2176	1870.5
	K00171	*porD*	968	1030	1711	1628.5
	K03737	*por*	34863.83	29371.36	34888.85	37464.21
	K11533	*fas*	482.33	309.33	274.66	383
	K00648	***fabH***	**37822.91**	**39201.94**	**39450.17**	**38731.79**
	K01962	*accA*	22029.05	20364.57	21357.08	22740.64
	K02160	*accB*	23614.05	23791.47	25778.98	25865.64
Fatty acid	K01963	*accD*	23401.55	21667.07	22187.08	23663.14
biosynthesis	K01961	*accC*	25561.8	26249.82	25471.33	24746.89
	K11263	*bccA*	3157.33	2133.33	1959.16	2843
	K18472	*accD6*	607.5	409	354	495
	K02372	*fabZ*	23578.71	22680.05	25870.55	26546.47
	K16363	*lpxC-fabZ*	4429.08	7024.74	5401.4	3427.75
	K01847	*mut*	12320.62	16620.18	12995.21	9919.42
	K01849	*mcmA2*	13711.5	10477.85	11543.68	14169.42
	K01848	*mcmA1*	14193.5	10820.85	11969.68	14602.42
Propanoate	K05606	*mcee*	19161.25	18578.6	17578.76	18242.17
metabolism	K01965	*pcca*	1487.42	1157.58	1052.58	1320.42
	K01966	*pccb*	7496.67	9767.43	7520.93	5891.67
	K01026	***pct***	**893.61**	**1095.38**	**818.61**	**930.73**
	K01905	***acdA***	**414**	**397**	**287**	**470**
Butanoate	K00626	*atoB*	43419.85	44255.99	30810.99	33626.42

metabolism	K00074	*paaH*	17667.83	18499.93	13835.04	14402.86
	K01692	*paaF/echA*	15303.2	11571.18	9974.05	14401.5
	K01825	*fadB*	2172.53	2439.6	26.8	28.83
	K01782	*fadJ*	3894.78	3697.67	1201.87	1566.08
	K01715	***crt***	**8238.77**	**8733.48**	**8259.54**	**8751.73**
	K17829	*ccrA*	957	721	455	739
	K00209	*fabV/ter*	57.25	132	38.5	54.25
	K00248	*bcd*	21589.63	18506.27	19868.55	22319.13
	K00634	***ptb***	**28863.94**	**22775.55**	**27374.28**	**30543.56**
	K00929	*buk*	31886.8	24822.74	30414.48	34162.19
	K13788	*pta*	3490.36	3488.93	730.63	919.33
Acetata	K00625	*pta*	10276.11	10280.21	11136.1	10037.07
oxidation	K00925	*ak*	28812.3	26697.65	28497.65	29308.23
	K15024	***pta***	**11636.25**	**8107.85**	**10624.6**	**12828.25**

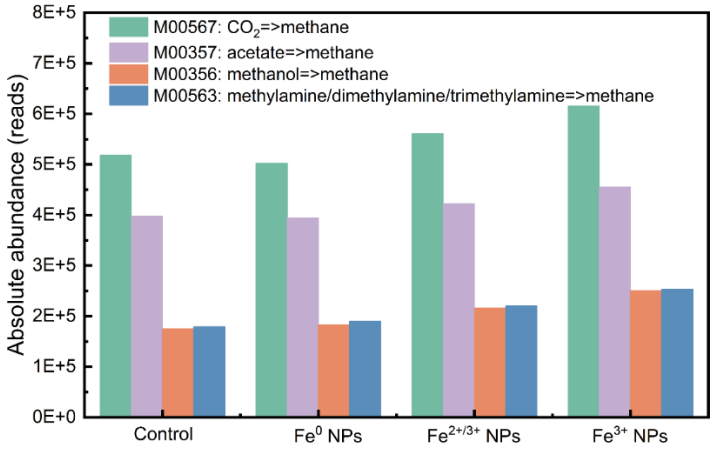

Fig. S4. the abundance of genes that encoded the key enzymes in Co-digestion with Fe NPs materials.

Table S5. The typical genes involved in methane metabolism and their abundance based on KEGG

Module	EC Number	KO Number	Gene name	Abundance (reads)			
				Control	Fe^0 NPs	$Fe^{2+/3+}$ NPs	Fe^{3+} NPs
M00567	1.2.7.12	K00200	*fwdA*	15754.34	17031.16	14701.16	14212.84
		K00201	*fwdB*	23377.18	23582.82	18314.32	15918.18
		K00202	*fwdC*	30617.51	26810.49	28177.99	27877.51
		K00203	*fwdD*	23317.51	23536.49	18012.99	15460.51
		K00205	*fwdF*	16142.51	14473.49	**22445.99**	**26888.51**
		K11260	*fwdG*	11696.67	10248.83	**12607.83**	**13672.17**
		K11261	*fwdE*	44033.34	37490.66	42863.16	**50344.34**
	2.3.1.101	K00672	*ftr*	19805.17	**20704.33**	**23603.83**	**26096.67**
	3.5.4.27	K01499	*mch*	11789.67	10534.83	**12881.83**	**13777.17**
	1.5.98.1	K00319	*mtd*	11696.67	10248.83	**12607.83**	**13672.17**
	1.5.98.2	K00320	*mer*	15777.67	17261.83	14652.83	13828.17
	1.12.98.1	K00440	*frhA*	4206.84	3816.16	**9750.66**	**13181.84**
		K00441	*frhB*	31523.85	31302.65	**36951.15**	**40342.35**
		K00442	*frhD*	4170.17	3779.83	**9523.33**	**12803.17**
		K00443	*frhG*	4206.84	3816.16	**9750.66**	**13181.84**
M00357	2.7.2.1	K00925	*ackA*	36.67	36.33	**227.33**	**378.67**
	2.3.1.8	K00625	*pta*	36.67	36.33	**227.33**	**378.67**
	6.2.1.1	K01895	*acs*	53766.67	50591.33	45473.33	41546.67
M00356	2.1.1.246	K14080	*mtaA*	380.01	364.49	**989.49**	**1293.51**
	2.1.1.90	K04480	*mtaB*	296.01	289.99	**908.99**	**1251.01**
		K14081	*mtaC*	389.01	380.49	**1018.49**	**1306.51**
M00563	2.1.1.247	K14082	*mtbA*	120.67	110.83	**299.83**	**417.17**
	2.1.1.250	K14083	*mttB*	166.34	163.16	**572.16**	**816.84**
		K14084	*mttC*	4248.34	6966.66	2427.66	936.34

2.1.1.249	K16178	*mtbB*	397.02	382.98	**1553.98**	**2370.02**
	K16179	*mtbC*	213.67	201.33	**417.33**	**476.67**
2.1.1.248	K16176	*mtmB*	416.68	400.82	**1216.82**	**1672.18**
	K16177	*mtmC*	241.34	221.66	**599.66**	**834.34**

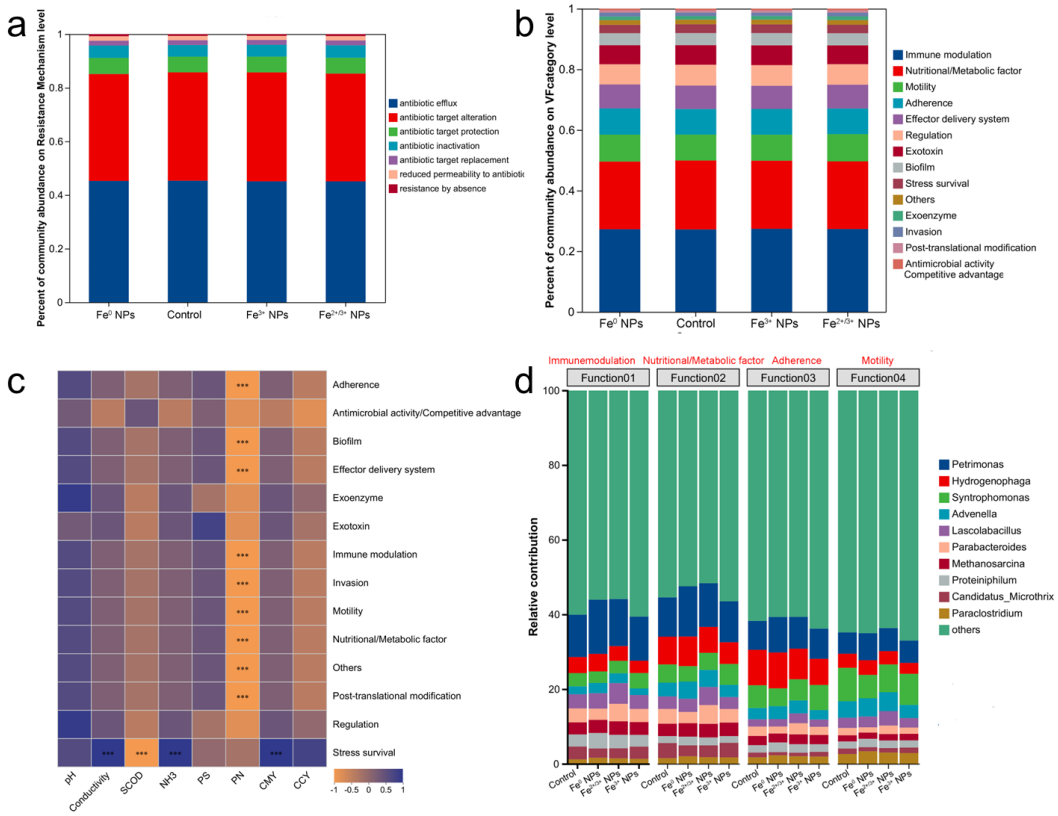

Fig. S5. (a) community bar plot based on resistance mechanism level; (b) community bar plot on the VF category of the top 20 species; (c) Spearman correlation heatmap on VF category level; (d) bar plot of species and functional contribution on VF category level.

Test S9. Practical feasibility and environmental implications of Fe NPs application in Co-AD systems

Although the Fe-NP concentration applied in this study (200 mg/L) proved effective in enhancing methane production and microbial functionality, its feasibility in full-scale applications warrants careful consideration. From a practical perspective, this dosage was selected based on prior literature demonstrating its utility in mechanistic investigations without inducing severe toxicity under controlled conditions (Zheng et al., 2023b; Wang et al., 2025). Recent research has further validated the feasibility of even higher doses: He et al. (2021) reported that 800 mg/L of nano-Fe_3O_4 effectively mitigated membrane fouling through bio-electrochemical effects rather than mere physical adsorption, enhancing MBR effluent quality (He et al., 2021a). Similarly, Liu et al. (2018) demonstrated that 1 g/L of magnetic iron powder exerted limited effects via adsorption or flocculation, but substantially delayed fouling due to magnetically induced microbial responses (Liu et al., 2018). These studies suggest that Fe-based nanomaterials can function effectively at higher concentrations through bio-functionality and redox interactions, and not solely by surface adsorption. However, for large-scale anaerobic digestion systems, such concentrations may pose challenges in terms of cost, nanoparticle sourcing, and potential accumulation. Economically, strategies such as periodic dosing, use of industrial Fe-rich byproducts (e.g., iron sludge, mill scale), or coupling with magnetic separation technologies could mitigate costs while retaining performance benefits (Huang et al., 2019; Hu et al., 2021).

Environmentally, Fe-NPs are likely to undergo transformation and aggregation under anaerobic, reductive conditions, forming less bioavailable species that predominantly settle into the sludge phase (Liu et al., 2024; Hoffmann et al., 2022). As such, their long-term fate and risk of release into downstream ecosystems remain areas of concern (Brar et al., 2010). Future work should thus incorporate life-cycle cost assessments and long-term ecotoxicological evaluations. Overall, while Fe-NPs show promise as redox-active additives for enhancing Co-AD efficiency, their dosage and fate must be optimized to ensure environmental safety and economic viability in full-scale operations.

Table S6. Comparison of CMY with recent Fe-based nanoparticle-enhanced AD studies

Substrate	Fe-based Type	Fe-based Dosage	Methane Yoeld	Increased vs. Control	Study
AFR+WAS	Fe^{3+} NPs	0.2 g/L	145.27 ± 10.48; Pm=163.64 ± 11.78 mL/g VS)	46.43%	This study
Sodium Propionate	Fe_3O_4 NPs	0.4 g/L	127.04±1.24 mL/g VS (Pm)	40.14%	(Wang et al., 2025)
WAS	Residual ferric ions	0.125 mmol/g VSS	92.51 mL/g VSS	29.3%	(He et al., 2021b)
WAS	Fe_2O_3	8.2 g/L	156.1 ± 9.9 mL/g-COD	20%	(Yang et al., 2024)
WAS	Magnetite	10 g/L	193.20 ± 1.98 mL/g-COD (Pm)	10.4%	(Zhu et al., 2023)

References

Andronikou M, Christoforou P, Constantinou D, Charalambous P, G. Samanides C, Karachaliou P, Vyrides I (2025) Critical role of bicarbonate in Zero-Valent iron for hydrogen generation and biogas upgrading in anaerobic digestion. Bioresource Technology, 426: 132236.

Aziz A, Sengar A, Basheer F, Farooqi I H, Isa M H (2022) Anaerobic digestion in the elimination of antibiotics and antibiotic-resistant genes from the environment – A comprehensive review. Journal of Environmental Chemical Engineering, 10: 106423.

Bennett B D, Gralnick J A (2019) Mechanisms of toxicity by and resistance to ferrous iron in anaerobic systems. Free Radical Biology and Medicine, 140: 167-171.

Brar S K, Verma M, Tyagi R D, Surampalli R Y (2010) Engineered nanoparticles in wastewater and wastewater sludge – Evidence and impacts. Waste Management, 30: 504-520.

Carrère H, Dumas C, Battimelli A, Batstone D J, Delgenès J P, Steyer J P, Ferrer I (2010) Pretreatment methods to improve sludge anaerobic degradability: A review. Journal of Hazardous Materials, 183: 1-15.

Chen C, Hall S J, Coward E, Thompson A (2020) Iron-mediated organic matter decomposition in humid soils can counteract protection. Nature Communications, 11: 2255.

Cheng Q, Huang W, Jiang M, Xu C, Fan G, Yan J, Chai B, Zhang Y, Zhang Y, Zhang S, Xiao B, Song G (2021) Challenges of anaerobic digestion in China. International Journal of Environmental Science and Technology, 18: 3685-3696.

Fan X, Zhang Z, Li N, Li X (2024) Molecular ecological insights into the synergistic response mechanism of nitrogen transformation, electron flow and antibiotic resistance genes in aerobic activated sludge systems driven by sulfamethoxazole and/or trimethoprim stresses. Water Research, 270: 122853.

Feng Y, Zhang Y, Quan X, Chen S (2014) Enhanced anaerobic digestion of waste activated sludge digestion by the addition of zero valent iron. Water Research, 52: 242-250.

He C S, He P P, Yang H Y, Li L L, Lin Y, Mu Y, Yu H Q (2017) Impact of zero-valent iron

nanoparticles on the activity of anaerobic granular sludge: From macroscopic to microcosmic investigation. Water Research, 127: 32-40.

He H, Xin X, Qiu W, Li D, Liu Z, Ma J (2021a) Role of nano-Fe_3O_4 particle on improving membrane bioreactor (MBR) performance: Alleviating membrane fouling and microbial mechanism. Water Research, 209: 117897.

He Z W, Yang C X, Tang C C, Liu W Z, Zhou A J, Ren Y X, Wang A J (2021b) Response of anaerobic digestion of waste activated sludge to residual ferric ions. Bioresource Technology, 322: 124536.

Hoffmann N, Fincheira P, Tortella G, Rubilar O (2022) The role of iron nanoparticles on anaerobic digestion: mechanisms, limitations, and perspectives. Environmental Science and Pollution Research, 29: 82619-82631.

Hu Z, Duan H, Wang Z, Zhao J, Ye L, Yuan Z, Zheng M, Hu S (2021) Centralized iron-dosing into returned sludge brings multifaceted benefits to wastewater management. Water Research, 203: 117536.

Huang S, Shi X, Bi X, Lee L Y, Ng H Y (2019) Effect of ferric hydroxide on membrane fouling in membrane bioreactor treating pharmaceutical wastewater. Bioresource Technology, 292: 121852.

Huang X, Miao X, Chu X, Luo L, Zhang H, Sun Y (2023) Enhancement effect of biochar addition on anaerobic co-digestion of pig manure and corn straw under biogas slurry circulation. Bioresource Technology, 372: 128654.

Jiang L, Dang Q, Zhao X, Zhang C, Tan X, Yan Q (2022) Mechanism of microbial involvement in nitrogen conversion affecting methane production in dry anaerobic digestion. Journal of Cleaner Production, 369: 133324.

Li P, Liu Z, Zhao M, Miao H, Shi W, Huang Z, Ruan W (2021a) Enhanced Methane Generation from Anaerobic Tridigestion of Organic Solid Wastes by Direct Interspecies Electron Transfer Stimulation. ACS Sustainable Chemistry & Engineering, 9: 12323-12331.

Li Y, Ni J, Cheng H, Zhu A, Guo G, Qin Y, Li Y Y (2021b) Methanogenic performance and microbial community during thermophilic digestion of food waste and sewage sludge in a high-solid anaerobic membrane bioreactor. Bioresource Technology, 342: 125938.

Liang L, Jin Z, Tao Y, Li Y, Zhao Z, Zhang Y (2024) Enhanced Extracellular Electron Transfer in Magnetite-Mediated Anaerobic Oxidation of Methane Coupled to Humic Substances Reduction: The Pivotal Role of Membrane-Bound Electron Transfer Proteins. Environmental Science & Technology, 58: 17756–17765.

Lim J W, Chiam J A, Wang J Y (2014) Microbial community structure reveals how microaeration improves fermentation during anaerobic co-digestion of brown water and food waste. Bioresource Technology, 171: 132-8.

Liu H, Xu Y, Li L, Li X, Dai X (2024) Enhancing proton-coupled electron transfer drives efficient methanogenesis in anaerobic digestion. Water Research, 266: 122331.

Liu H, Xu Y, Li L, Yuan S, Geng H, Tang Y, Dai X (2022) A novel green composite conductive material enhancing anaerobic digestion of waste activated sludge via improving electron transfer and metabolic activity. Water Research, 220: 118687.

Liu L, Chen Y, Qi J, Sun J, Zhang L (2025) The role of sulfidated zero-valent iron in enhancing anaerobic digestion of waste activated sludge. Journal of Environmental Management, 375: 124283.

Liu Y, Liu Q, Li J, Ngo H H, Guo W, Hu J, Gao M-t, Wang Q, Hou Y (2018) Effect of magnetic powder on membrane fouling mitigation and microbial community/composition in membrane bioreactors (MBRs) for municipal wastewater treatment. Bioresource Technology, 249: 377-385.

Liu Y, Xiao Q, Ye X, Wang C, Jia Z, Du J, Kong X, Xi Y (2021a) Effect of different charged Fe_3O_4 nanoparticles on methane production for anaerobic digestion of wheat straw. Journal of Cleaner Production, 328: 129655.

Liu Z, Zhou A, Wang S, Cheng S, Yin X, Yue X (2021b) Quorum sensing shaped microbial consortia and enhanced hydrogen recovery from waste activated sludge electro-fermentation on basis of free nitrous acid treatment. Science of the Total Environment, 766: 144348.

Lu Y, Zhou X, Zheng Y, Yang H, Cao W (2025) How far do we still need to go with antibiotics in aquatic environments? Antibiotic occurrence, chemical-free or chemical-limited strategies, key challenges, and future perspectives. Water Research, 275: 123179.

Lyu Z, Shao N, Akinyemi T, Whitman W B (2018) Methanogenesis. Current Biology, 28:

727-732.

Mortezaei Y, Williams M R, Demirer G N (2024) The fate of antibiotic resistance genes during anaerobic digestion of sewage sludge with ultrasonic pretreatment. Environmental Science and Pollution Research, 31: 5513-5525.

Peng H, Zhang Y B, Tan D M, Zhao Z Q, Zhao H M, Quan X (2018) Roles of magnetite and granular activated carbon in improvement of anaerobic sludge digestion. Bioresource Technology, 249: 666-672.

Qin Y, Wang H, Li X, Cheng J J, Wu W (2017) Improving methane yield from organic fraction of municipal solid waste (OFMSW) with magnetic rice-straw biochar. Bioresource Technology, 245: 1058-1066.

Rani J, Pandey K P, Kushwaha J, Priyadarsini M, Dhoble A S (2022) Antibiotics in anaerobic digestion: Investigative studies on digester performance and microbial diversity. Bioresource Technology, 361: 127662.

Shi L, Dong H, Reguera G, Beyenal H, Lu A, Liu J, Yu H Q, Fredrickson J K (2016) Extracellular electron transfer mechanisms between microorganisms and minerals. Nature Reviews Microbiology, 14: 651-62.

Tang Z, Huang C, Tian Y, Xi B, Guo W, Tan W (2021) Fate of antibiotic resistance genes in industrial-scale rapid composting of pharmaceutical fermentation residue: The role implications of microbial community structure and mobile genetic elements. Environmental Pollution, 291: 118155.

Tao N, Xu M, Wu X, Pi Z, Yu C, Fang D, Zhou L (2021) Supplementation of Schwertmannite improves methane production and heavy metal stabilization during anaerobic swine manure treatment. Fuel, 299: 120883.

Wang B, Xu Z, Dong B (2024a) Occurrence, fate, and ecological risk of antibiotics in wastewater treatment plants in China: A review. Journal of Hazardous Materials, 469: 133925.

Wang D, Pan Q, Yang J, Gong S, Liu X, Fu Y (2024b) Effects of Mixtures of Engineered Nanoparticles and Cocontaminants on Anaerobic Digestion. Environmental Science & Technology, 58: 2598-2614.

Wang F, Song G, Zhang M, Zhao S, Wang T, Zhao K, Wang X, Liu R (2025) Fe3O4

nanoparticles promote methanogenesis in propionate acclimated system. Bioresource Technology, 431: 132608.

Wang H, Sun H, Ren H, Cao G, Xie G, Xing D, Ren N, Liu B (2023a) Metagenomic reveals the methanogenesis metabolic mechanism of high-solids anaerobic digestion of human feces under gradient domestication. Chemical Engineering Journal, 460: 141752.

Wang J, Lou Y, Ma D, Feng K, Chen C, Zhao L, Xing D (2023b) Co-treatment with free nitrous acid and calcium peroxide regulates microbiome and metabolic functions of acidogenesis and methanogenesis in sludge anaerobic digestion. Science of the Total Environment, 870: 161924.

Wang M, Ren T, Yin M, Lu K, Xu H, Huang X, Zhang X (2023c) Enhanced anaerobic wastewater treatment by a binary electroactive material: pseudocapacitance/conductance-mediated microbial interspecies electron transfer. Environmental Science & Technology, 57: 12072-12082.

Xiao K K, Yu Z C, Pei K Y, Sun M, Zhu Y W, Liang S, Hou H J, Liu B C, Hu J P, Yang J K (2022) Anaerobic digestion of sludge by different pretreatments: Changes of amino acids and microbial community. Frontiers of Environmental Science & Engineering, 16(2): 23.

Xu H, Wang M, Hei S, Qi X, Zhang X, Liang P, Fu W, Pan B, Huang X (2024) Neglected role of iron redox cycle in direct interspecies electron transfer in anaerobic methanogenesis: Inspired from biogeochemical processes. Water Research, 262: 122125.

Yamada T, Sekiguchi Y, Imachi H, Kamagata Y, Ohashi A, Harada H (2005) Diversity, localization, and physiological properties of filamentous microbes belonging to Chloroflexi subphylum I in mesophilic and thermophilic methanogenic sludge granules. Applied and Environmental Microbiology, 71: 7493-503.

Yan B, Chen X, Wang Z, Li J, Li T, Mu L, Chen G (2025) Anaerobic co-digestion of antibiotic fermentation residues and corn stalks for biogas production and elimination of antibiotic resistance genes. Fuel, 387: 134442.

Yang G, Wang J (2019) Changes in microbial community structure during dark fermentative hydrogen production. International Journal of Hydrogen Energy, 44: 25542-25550.

Yang Y, Cheng X, Rene E R, Qiu B, Hu Q (2024) Effect of iron sources on methane production and phosphorous transformation in an anaerobic digestion system of waste

activated sludge. Bioresource Technology, 395: 130315.

Ye J, Hu A, Cheng X, Lin W, Liu X, Zhou S, He Z (2018a) Response of enhanced sludge methanogenesis by red mud to temperature: Spectroscopic and electrochemical elucidation of endogenous redox mediators. Water Research, 143: 240-249.

Ye J, Hu A, Ren G, Chen M, Tang J, Zhang P, Zhou S, He Z (2018b) Enhancing sludge methanogenesis with improved redox activity of extracellular polymeric substances by hematite in red mud. Water Research, 134: 54-62.

Yin Q, Yang S, Wang Z, Xing L, Wu G (2018) Clarifying electron transfer and metagenomic analysis of microbial community in the methane production process with the addition of ferroferric oxide. Chemical Engineering Journal, 333: 216-225.

Yin Y, Lou T, Song W, Wang C, Wang J (2023) Production of medium chain fatty acids from fermentation of antibiotic residuals: Fate of antibiotic resistance genes. Bioresource Technology, 379: 129056.

Ying G G, He L Y, Ying A J, Zhang Q Q, Liu Y S, Zhao J L (2017) China Must Reduce Its Antibiotic Use. Environmental Science & Technology, 51: 1072-1073.

Zhang J, You Z, Liu D, Tang R, Zhao C, Cao Y, Li F, Song H (2023a) Conductive proteins-based extracellular electron transfer of electroactive microorganisms. Quantitative Biology, 11: 405-420.

Zhang X, Jiao P, Zhang M, Wu P, Zhang Y, Wang Y, Xu K, Yu J, Ma L (2023b) Impacts of organic loading rate and hydraulic retention time on organics degradation, interspecies interactions and functional traits in thermophilic anaerobic co-digestion of food waste and sewage sludge. Bioresource Technology, 370: 128578.

Zhang Z, Guo L, Wang Y, Li F, Zhao Y, Gao M, She Z (2017) Degradation and transformation of extracellular polymeric substances (EPS) and dissolved organic matters (DOM) during two-stage anaerobic digestion with waste sludge. International Journal of Hydrogen Energy, 42: 9619-9629.

Zhang Z, Zhang Z, Zhang C, Chang Q, Fang Q, Liao C, Chen J, Alvarez P J J, Chen W, Zhang T (2024) Simultaneous Reduction and Methylation of Nanoparticulate Mercury: The Critical Role of Extracellular Electron Transfer. Environmental Science & Technology, 58: 18368-18378.

Zhao Q, Guo W, Luo H, Xing C, Wang H, Liu B, Si Q, Ren N (2021) Deciphering the transfers of antibiotic resistance genes under antibiotic exposure conditions: Driven by functional modules and bacterial community. Water Research, 205: 117672.

Zhao Z, Wang J, Li Y, Zhu T, Yu Q, Wang T, Liang S, Zhang Y (2020) Why do DIETers like drinking: Metagenomic analysis for methane and energy metabolism during anaerobic digestion with ethanol. Water Research, 171: 115425.

Zhao Z, Zhang Y, Li Y, Quan X, Zhao Z (2018) Comparing the mechanisms of ZVI and Fe_3O_4 for promoting waste-activated sludge digestion. Water Research, 144: 126-133.

Zhao Z, Zhang Y, Yu Q, Dang Y, Li Y, Quan X (2016) Communities stimulated with ethanol to perform direct interspecies electron transfer for syntrophic metabolism of propionate and butyrate. Water Research, 102: 475-484.

Zhen G, Zheng S, Han Y, Zhang Z, Lu X, Xu K (2022) Semi-continuous anolyte circulation to strengthen CO2 bioelectromethanosynthesis with complex organic matters as the e-/H+ donor for simultaneous biowaste refinery. Chemical Engineering Journal, 430: 133123.

Zheng M, Ou H, Dong F, He C, Hu Z, Wang W (2023a) Mechanism insights into enhanced treatment of wasted activated sludge by hydrogen-mediated anaerobic digestion. Environmental Science and Pollution Research, 30: 47787-47799.

Zheng N, Sun X, Shi Y, Chen L, Wang L, Cai H, Han C, Liao T, Yang C, Zuo Z, He C (2023b) The valence state of iron-based nanomaterials determines the ferroptosis potential in a zebrafish model. Science of the Total Environment, 855: 158715.

Zhong Y, He J, Zhang P, Zou X, Pan X, Zhang J (2022) Effects of different particle size of zero-valent iron (ZVI) during anaerobic digestion: Performance and mechanism from genetic level. Chemical Engineering Journal, 435: 134977.

Zhu D, Wang Z, Liu K, Si B, Yang G, Tian C, Zhang Y (2023) Multi-cycle anaerobic digestion of hydrothermal liquefaction aqueous phase: Role of carbon and iron based conductive materials in inhibitory compounds degradation, microbial structure shaping, and interspecies electron transfer regulation. Chemical Engineering Journal, 454: 140019.

Zhu L, Wu B, Liu Y, Zhang J, Deng R, Gu L (2022) Strategy to enhance semi-continuous anaerobic digestion of food waste by combined use of calcium peroxide and magnetite.

Water Research, 221: 118801.

Zhu R, Chen Y, Zhao T, Jiang Q, Wang H, Zheng L, Shi D, Zhai J, He Q, Gu L (2020) Enhanced mesophilic anaerobic co-digestion of waste sludge and food waste by using hematite (α-Fe2O3) supported bentonite as additive. Bioresource Technology, 313: 123603.

Ziganshina E E, Belostotskiy D E, Bulynina S S, Ziganshin A M (2021) Effect of magnetite on anaerobic digestion of distillers grains and beet pulp: Operation of reactors and microbial community dynamics. Journal of Bioscience and Bioengineering, 131: 290-298.